A new approach to estimate ice dynamic rates using satellite observations in East Antarctica

Bianca Kallenberg[1], Paul Tregoning[1], Janosch F. Hoffmann[2], Rhys Hawkins[1], Anthony Purcell[1], Sébastien Allgeyer[1]

[1]Research School of Earth Sciences, Australian National University, Canberra, ACT, 0200, Australia
[2]College of Computer, Mathematical, and Natural Science, University of Maryland, College Park, MD 20742, USA

Correspondence to: Bianca Kallenberg (bianca.kallenberg@anu.edu.au)

Abstract.

Mass balance changes of the Antarctic ice sheet are of significant interest due to its sensitivity to climatic changes and its contribution to changes in global sea level. While regional climate models successfully estimate mass input due to snowfall, it remains difficult to estimate the amount of mass loss due to ice dynamic processes. It's often been assumed that changes in ice dynamic rates only need to be considered when assessing long term ice sheet mass balance; however, two decades of satellite altimetry observations reveal that the Antarctic ice sheet changes unexpectedly and much more dynamically than previously expected. Despite available estimates on ice dynamic rates obtained from radar altimetry, information about ice sheet changes due to changes in the ice dynamic are still limited, especially in East Antarctica. Without understanding ice dynamic rates it is not possible to properly assess changes in ice sheet mass balance, surface elevation or to develop ice sheet models. In this study we investigate the possibility of estimating ice sheet changes due to ice dynamic rates by removing modelled rates of surface mass balance, firn compaction and bedrock uplift from satellite altimetry and gravity observations. With similar rates of ice discharge acquired from two different satellite missions we show that it is possible to obtain an approximation of the rate of change due to ice dynamics by combining altimetry and gravity observations. Thus, surface elevation changes due to surface mass balance, firn compaction and ice dynamic rates can be modelled and correlate with observed elevation changes from satellite altimetry.

1 Introduction

Assessing and understanding ice mass balance of the Antarctic Ice Sheet (AIS) is challenging due to the remoteness and extensive ice cover of the continent, resulting in a sparse network of field observations to provide information about the climate, mass balance and bedrock uplift rates. In order for an ice sheet to be in balance, the amount of ice lost due to the dynamic processes of meltwater runoff and solid ice discharge over the grounding line, needs to be balanced by accumulated snowfall. If one exceeds the other, the ice sheet either gains or loses mass, resulting in a change in ice sheet mass balance (Cuffey and Paterson, 2010). The surface processes of snowfall, snowmelt and subsequent runoff, sublimation, evaporation and snowdrift add, remove or distribute snow and define the surface mass balance (SMB) (e.g. Lenaerts et al., 2012; Van Wessem et al., 2014). Changes in SMB occur primarily in the firn layer that covers the AIS, the intermediate product between snow and ice (Ligtenberg et al., 2011). Temperature variations, overburden pressure, deformation and repositioning of snow grains causes snow to densify until it reached the density of glacier ice ($\sim$917 kg m^{-3}) (Herron and Langway, 1980). The intermediate product is called firn, and changes in SMB occur primarily in the firn layer that covers the AIS (Ligtenberg et al., 2011). This results in a change in the ice sheet surface elevation without changing the mass of the ice sheet.

When thoroughly evaluated with field observations and downscaled using statistical interpolation methods, regional climate models can be used to simulate fields of SMB components, temperature and near-surface wind speed. Ice loss rates can be obtained by combining individual estimates of accumulation, ablation and dynamic ice loss, with the difference between mass input and mass output providing the mass balance of the ice sheet. While SMB can be taken from regional climate models, estimates on ice discharge are limited and difficult to obtain. The amount of ice discharge can be estimated by obtaining the product of ice velocity and ice thickness across the grounding-line. Satellite radar interferometry is used to retrieve information about ice velocity rates. The ice thickness is estimated from airborne radar or, in the absence of direct observations, using surface elevation observations under the assumption that the ice is floating once it has crossed the grounding line (Rignot and Thomas, 2002; Rignot et al., 2008; Allison et al., 2009). Commonly, changes due to ice dynamics are either taken from these by satellite altimetry derived estimates (Shepherd et al., 2012; Sasgen et al.,

2013), or assumed to be insignificant when studying short-term changes (e.g. Ligtenberg et al., 2011). However, unexpected changes in ice sheet dynamic have been observed in the past decades, with some glaciers found to accelerate, while others decelerated (Rémy and Frezzotti, 2006). In general, ice dynamics are not well known and information about ice dynamic variations are limited (Rignot, 2006;

5   Rignot et al., 2008). This becomes an issue when assessing ice mass balance and surface elevation changes, or establishing ice sheet models.

Although satellite observations help provide information about temporal and spatial changes in ice mass and ice volume, large uncertainties remain when interpreting the signals and assigning the origin of change. Ice mass balance can be measured directly from gravity observations but needs to be separated

10   into the possible changes caused by SMB, ice dynamics and Glacial Isostatic Adjustment (GIA), which is the response of the lithosphere to changes in surface loading. Changes in ice sheet thickness can be obtained from altimetry observations but need to be separated into the change caused by SMB, ice dynamics, GIA and/or firn compaction. Observed elevation changes can subsequently be converted to changes in mass by employing firn densities.

15   In this study we obtain an estimate of ice sheet changes due to ice dynamic rates by combining modelled SMB rates using the Regional Atmospheric Climate MOdel (RACMO2), Gravity Recovery And Climate Experiment (GRACE) and laser altimetry observations from the Ice, Cloud and land Elevation Satellite (ICESat). We found that the attained estimates of ice dynamic changes obtained from GRACE and ICESat are of similar magnitude. In conjunction with our estimates on our rate of change

20   due to ice dynamics we model the rate of change of the ice surface and compare our results with direct observations taken from ICESat measurements. A study site in East Antarctica has been chosen due to the increase in mass that has been observed there by GRACE and altimetry, suggesting a thickening of the ice sheet.

2 Study area

25   The chosen study area combines Enderby Land, Kemp Land and MacRobertson Land, and parts of Dronning Maud Land and Princess Elizabeth Land (hereafter referred to as Enderby Land for simplicity). The study area is assumed to be a stable region (e.g. Rignot et al., 2008), with the ice sheet

predominantly located on bedrock above sea level, making it less vulnerable to changes in ocean temperatures. The major outlet glaciers of this region are the Lambert and Mellor glaciers feeding the Amery Ice Shelf in the east, together with the smaller (~3000 km^2) Fisher, Scylla and American Highland Glaciers. Only smaller glaciers are found along the remaining coastal region of Enderby Land,

5   including the Shirase, Rayner, Thyer and Robert glaciers (Fig. 1). Previous research based on the mass budget method found the ice sheet to be largely in balance across this area, possibly even slightly thickening (Rignot, 2006; Rignot et al., 2008; Rignot et al., 2013). A general positive mass trend across this region has also been recorded by gravity and altimetry observations (e.g. Shepherd et al., 2012; Sasgen et al., 2013).

10   **3 Data sets and implemented models**

We use observational measurements of mass variations from the Gravity Recovery And Climate Experiment (GRACE) and surface elevation changes observed by laser altimetry using the Ice, Cloud and land Elevation Satellite (ICESat). The regional climate model RACMO2/ANT is used to model the trend in SMB and to force the firn compaction model. Two versions of the RACMO2 model are used

15   here, RACMO2.1 and RACMO2.3. The SMB used throughout this paper is the sum of snowfall, evaporation/sublimation, snowdrift and runoff. The SMB components are provided in kg m^{-2} t^{-1}, where t is the temporal resolution of the model.

3.1 GRACE

We use the monthly gravity field solutions CNES/GRGS RL03-v3, provided by the Groupe de

20   Researches de Géodésie Spatiale (GRGS). The RL03 solutions have a spatial resolution of degree and order 80 (Lemoine et al., 2013) and have been chosen due to the stabilisation process that is applied to reduce noise in form of North-South striping. This is achieved by regularising the inversion for spherical harmonic coefficients (Bruinsma et al., 2010).

Temporary changes in the Earth's gravity field can be related to changes in surface mass due to the

25   distribution of mass, as well as the elastic and viscoelastic (GIA) response of the lithosphere, the instantaneous and long term signal to changes in surface load (Wahr et al., 1998). We obtain mass

anomalies by applying the equations that relate mass changes to gravity changes (Wahr et al., 1998) to obtain the change in mass due to SMB:

$$U^{w.e.}(\theta,\lambda,t) = R \sum_{n=2}^{N} \sum_{m=0}^{n} P_{nm}(\cos\theta) \frac{2n+1}{1+k_n^{elast}} \left(\Delta C_{nm}(t)\cos m\lambda + \Delta S_{nm}(t)\sin m\lambda \right) \qquad (1)$$

5

and due to the viscoelastic deformation, or GIA:

$$U^{visco}(\theta,\lambda,t) = R \sum_{n=2}^{N} \sum_{m=0}^{n} P_{nm}(\cos\theta) \frac{h_n^{visco}}{k_n^{visco}} \left(\Delta C_{nm}(t)\cos m\lambda + \Delta S_{nm}(t)\sin m\lambda \right) \qquad (2)$$

10 where R is the Earth's radius, P_{nm} are the fully normalised Legendre functions, n and m are degree and order of the spherical harmonic coefficients, θ and λ are colatitude and longitude, and ΔC_{nm}, ΔS_{nm} are the spherical harmonic coefficients, at time t, of the GRACE anomaly fields. k_n and h_n are the elastic Love loading numbers (e.g. Pagiatakis, 1990) and the ratio of viscoelastic Love loading numbers (Purcell et al., 2011), depending on the degree. Purcell et al. (2011) showed that this empirical

15 approximation permitted the accurate computation of viscoelastic uplift that was independent of any particular GIA model, provided that there has been no change in load for the past 5000 years.

3.2. ICESat

Various methods are used to estimate surface elevation changes from ICESat observations, using either along-track measurements or measurements directly taken from the crossover location. Due to

20 perturbations in the orbit, deviations of the repeated ground track occur and it is necessary to determine the surface topography to correct elevation changes due to surface slope rather than changes in ice mass. Different methods have been applied to obtain surface elevation changes, using either along-track observations or crossover measurements (e.g. Slobbe et al., 2008; Gunter et al., 2009; Pritchard et al., 2009; Sørensen et al., 2011; Ewert et al., 2012).

25 Here we use the estimated rate of change of ice sheet elevation obtained from a newly developed

technique that combines both crossover and along-track observations (Hoffmann, 2016). The method allows estimation of the local surface slope using a digital elevation model that has been derived from gridded estimates of ice height at ICESat crossover points. Over a crossover grid that geographically spans all campaign crossovers of a location, a static grid was created on which heights were interpolated

5   at the epochs of all campaigns. The estimate of the elevation change over time is made by computing a weighted least-square regression of the height time series of each grid node and then computing a weighted mean value for all grid nodes to derive the crossover height rate. This not only allows to assess height rates at one location over time, but also to evaluate a digital elevation model directly from the data, which is used to estimate the slope at crossovers (Hoffman, 2016).

10 The slope estimates at the crossovers are then interpolated to remove the surface slope from the along-track measurements. Although the elevation change estimates from along-track measurements are naturally less precise than the rate estimates at crossovers, combining both methods significantly increases the accuracy of the slope correction, providing a measure to validate along-track estimates (Hoffman, 2016).

15 **3.3. RACMO2/ANT**

The RACMO2/ANT regional climate model, used to obtain SMB estimates, adopts the dynamical processes from the High Resolution Limited Area Model (HIRLAM) and the physical atmospheric processes from the European Centre for Medium-range Weather Forecasts (ECMWF) (Reijmer et al., 2005) and is forced by ERA-Interim reanalysis data at the lateral boundaries (e.g. Ligtenberg et al.,

20 2011; Lenaerts and van den Broeke, 2012). The latest version, RACMO2.3 (Van Wessem et al., 2014), extends available model data from 1979-2012 (RACMO2.1) to 1979-2015 (RACMO2.3) and improves the temporal resolution from 6-hourly (RACMO2.1) to 3-hourly (RACMO2.3) (Ligtenberg per. comm., 2016). The horizontal resolution is 27 km and the vertical resolution 40 levels. Individual SMB components are provided including snowfall, evaporation/sublimation, and snowmelt, as well as

25 snowdrift in RACMO2.3. Over Antarctica RACMO2/ANT is coupled with a multilayer snow model, which estimates meltwater percolation, refreezing and runoff, as well as surface albedo and snowdrift (Van Wessem et al., 2014). The update in the physical parameters of RACMO2.3 results in a general

6

increase in precipitation over the grounded East Antarctic Ice Sheet, evaluated using in-situ observations, ice-balance velocities and GRACE measurements and showing a general improvement of the SMB (Van Wessem et al., 2014).

3.4. Firn compaction

5   We developed a firn compaction model based on the firn densification model of Ligtenberg et al. (2011), using near surface climate provided by RACMO2.1. It is a one-dimensional, time-dependent model that estimates density and temperature individually for each layer and at each time step in a vertical firn column. The firn densification model of Ligtenberg et al. (2011) adds new snowfall instantly to the current top layer until the layer thickness exceeds ~15 cm (Ligtenberg, pers. comm.,

10   2016), at which time it is divided in two layers. The properties of each layer are passed on to both layers. If a layer becomes too thin, due to compaction or surface melt, the layer is merged with the next layer and assigned the average properties of both layers. Our model has been simplified to improve the computational time. Rather than adding new snowfall instantly to the top layer, we compute the monthly sum of SMB and use the monthly averaged surface temperature to estimate the densification

15   rate, density and new temperature to obtain the vertical velocity of the surface due to monthly firn compaction.

The model starts with a new firn layer created by the total SMB of one month and is built up by adding a new layer each month using monthly SMB values and mean surface temperatures. The surface snow density of each top layer is estimated using the proposed parameterisation of Kaspers et al. (2004),

20   together with a proposed slope correction to improve the fit in Antarctica by Helsen et al. (2008):

$$\rho_s = -151.94 + 1.4266(73.6 + 1.06T + 0.0669A + 4.77W) \qquad (3)$$

where T is the average annual temperature (in K), A the average annual accumulation (in mm water

25   equivalent (w.e.) yr^{-1}) and W the average annual wind speed 10m above the surface (in m s^{-1}). The densification rate is obtained using a dry snow densification expression proposed by Arthern et al. (2010):

7

$$\frac{d\rho}{dt} = CAg(\rho_i - \rho)e^{\left(\frac{-E_c}{RT} + \frac{-E_g}{RT_{av}}\right)}$$
(4)

where C is the grain-growth constant (m s^2 kg^{-1}), independently calculated for densities below (C = 0.07) and above (C = 0.03) the critical density of 550 kg m^{-3}, A is the accumulation rate (mm w.e. yr^{-1}), g the gravitational acceleration, and ρ and ρ_i are the local density and the ice density (kg m^{-3}), respectively. The exponential term includes the activation energy constants (kJ mol^{-1}) for creep and for grain-growth, E_c and E_g, respectively, the gas constant R (J mol^{-1} K^{-1}) and the local temperature T, and annual average temperature T_{av} (K).

The process of liquid water percolation and refreezing is incorporated as a function of snow porosity P_s and density, as proposed by Coléou and Lesaffre (1998) (Ligtenberg et al., 2011; Kuipers Munneke et al., 2015):

$$L_W = 1.7 + 5.7\left(\frac{P_S}{1 - P_S}\right)$$
(5)

with the snow porosity:

$$P_S = 1 - \left(\frac{\rho}{\rho_i}\right)$$
(6)

where ρ is the density of the layer and ρ_i the density of glacier ice.

The heat transport throughout the firn column is solved explicitly using the one-dimensional heat-transfer equation (Cuffey and Paterson, 2010):

$$\frac{dT}{dt} = \kappa \frac{d^2T}{dz^2}$$
(7)

8

with the thermal diffusivity κ and the depth z. Initially the heat-transfer equation consists of a term for heat conduction, advection and internal heating. However, initial heating is small within the firn layer and therefore neglected and the contribution of heat advection is taken into account by the downward motion of the ice flow (Cuffey and Paterson, 2010; Ligtenberg et al., 2011).

Finally, once the densification rate is estimated, the vertical velocity of the surface due to firn compaction, V_{fc}, can be assessed by integrating over the displacement of the compacted firn layers over the length of the firn column (Helsen et al., 2008):

$$V_{fc}(z,t) = \int_{z_i}^{z} \frac{1}{\rho(z)} \frac{d\rho(z)}{dt} dz \tag{8}$$

where z is depth, ρ density and $d\rho(z)/dt$ the densification rate.

Ligtenberg et al. (2011) found that Equation (4) over-predicts the rate of densification for most regions in Antarctica, with the effect of the annual average accumulation being too large on the densification rate. They reintroduced an accumulation constant that previously had been proposed by Herron and Langway (1980) as α in A^{α} (below 550 kg m^{-3}) and β in A^{β} (above 550 kg m^{-3}), initially chosen between 0.5 and 1.1 but later assumed to be α, β =1 (Zwally and Li, 2002; Helsen et al., 2008). Ligtenberg et al. (2011) applied a modelled to observed ratio to correct for the accumulation dependence. We also found that Equation (4) over-predicts the rate of densification, depending on the rate of the average annual accumulation.

However, due to our use of monthly layers, the ratio proposed by Ligtenberg et al. (2011) is no longer valid and we introduce new α and β, depending on the accumulation rate (Table A1). The values for α and β represent a best fit and have been obtained by investigating different values across several model runs. This means that the firn compaction model is adjusted to fit available observations and is therefore assumed to be correct and invariant of SMB model changes.

In Figure 2a we show the average annual rate of firn compaction across the study site and in Figure 2b

9

the differences between our model and the model of Ligtenberg et al. (2011). Along the ice sheet margins and the Amery Ice Sheet our model overestimates their firn compaction rates by 5-10 cm yr^{-1}, while it underestimates rates by 7-12 cm yr^{-1} in most other areas further inland, with up to 15 cm yr^{-1} at two individual location near 28°E and between 68°E and 70°E. These differences are within our

5   estimated uncertainty, based on the uncertainties provided for the modelled SMB from RACMO2 (Appendix A3).

4 Method to estimate the rate of change due to ice dynamic

A change in surface elevation, dH/dt, as measured by satellite altimetry is caused by a combination of processes that affect ice sheet thickness as well as the effect of GIA. The temporal change in surface

10   height can be described as:

$$\frac{dH^{ICESat}}{dt} = \frac{dH^{SMB}}{dt} + \frac{dH^{fc}}{dt} + \frac{dH^{ice}}{dt} + \frac{dH^{GIA}}{dt}$$ (9)

with the individual components representing elevation changes related to SMB (dH^{SMB}/dt), firn

15   compaction (dH^{fc}/dt), ice dynamics (dH^{ice}/dt), and the elastic and viscoelastic response of the lithosphere combined under the term of GIA (dH^{GIA}/dt). While the process of firn compaction plays an important role in surface elevation changes it does not affect the overall mass balance of the ice sheet. Therefore, the general change in ice mass as detected by GRACE can be expressed as:

20   $$\frac{dM^{GRACE}}{dt} = \frac{dM^{SMB}}{dt} + \frac{dM^{ice}}{dt} + \frac{dM^{GIA}}{dt}$$ (10)

with the individual components representing a change in mass due to SMB (dM^{SMB}/dt), ice dynamics (dM^{ice}/dt), and GIA (dM^{GIA}/dt).

25   With the components that assemble dM^{SMB}/dt being represented by regional climate models simulating

near surface climate in Antarctica, and dM^{GIA}/dt modelled by available GIA models, dM^{ice}/dt remains the only unknown in Equation 10. Therefore, an estimate of dM^{ice}/dt can be obtained by removing dM^{SMB}/dt and dM^{GIA}/dt from the GRACE observations:

$$5 \quad \frac{dM^{ice}}{dt} = \frac{dM^{GRACE}}{dt} - \frac{dM^{SMB}}{dt} - \frac{dM^{GIA}}{dt} \ . \tag{11}$$

Similarly, the same approach can be used to obtain dH^{ice}/dt from altimetry:

$$\frac{dH^{ice}}{dt} = \frac{dH^{ICESat}}{dt} - \frac{dH^{SMB}}{dt} - \frac{dH^{fc}}{dt} - \frac{dH^{GIA}}{dt} \ . \tag{12}$$

10

The solutions to Equation 10 and 11 are the changes in ice mass, $\frac{dM^{ice}_{GRACE}}{dt}$, and surface elevation, $\frac{dH^{ice}_{ICESat}}{dt}$, associated with changes in ice dynamics. We assume that changes within the firn layer have been taken into account by removing the rate of change due to SMB and firn compaction from the observations, and that the remaining signal is solely due to changes within the glacier ice. Therefore, we can convert

15 to/from the rate of change in mass and surface elevation by dividing/multiplying by the density of glacier ice. Thus, observations from each satellite mission can provide an independent estimate of the ice dynamics.

We first correct both observational measurements, GRACE and ICESat, for GIA using three available GIA models: the W12a model of Whitehouse et al. (2012), the ICE-6G_C (VM5a) model of Peltier et

20 al. (2015) and the recomputed version ICE6G_ANU of Purcell et al. (2016). Changes due to SMB are modelled using RACMO2.3/ANT, and the total trend due to SMB, for the period 2003-2009, is obtained using the monthly SMB (kg m^{-2} mth^{-1}). The change in dH^{SMB}/dt is acquired by dividing dM^{SMB}/dt by the density of surface snow (Eq.3), and the rate of change due to firn compaction, dH^{fc}/dt, is taken into account by using our modelled firn compaction rates. Each month, the total SMB is

25 computed and a monthly average firn compaction rate is removed from the SMB, before calculating the

overall trend dH^{SMB}/dt over 2003-2009. Finally, the obtained $\frac{dH^{ice}_{ICESat}}{dt}$ rates can be converted to $\frac{dM^{ice}_{ICESat}}{dt}$ by multiplying by the density of glacier ice (~ 917 kg m^{-3}), while the $\frac{dM^{ice}_{GRACE}}{dt}$ rates are converted to $\frac{dH^{ice}_{GRACE}}{dt}$ by dividing by the density of glacier ice.

If ICESat and GRACE detect the same signal, the obtained $\frac{dM^{ice}_{ICESat}}{dt}$ estimates should correlate with $\frac{dM^{ice}_{GRACE}}{dt}$ and vice versa, $\frac{dH^{ice}_{ICESat}}{dt}$ with $\frac{dH^{ice}_{GRACE}}{dt}$. Moreover, modelling surface elevation changes ($\frac{dH^{Mod}}{dt}$) found by removing $\frac{dH^{ice}_{GRACE}}{dt}$ from the modelled dH^{SMB}/dt and dH^{fc}/dt estimates should approximate the ICESat observations:

$$\frac{dH^{Mod}}{dt} = \left(\frac{dH^{SMB}}{dt} - \frac{dH^{fc}}{dt} \right) - \frac{dH^{GIA}}{dt} - \frac{dH^{ice}_{GRACE}}{dt}. \tag{13}$$

Conversely, $\frac{dH^{ice}_{ICESat}}{dt}$ not being equal to $\frac{dH^{ice}_{GRACE}}{dt}$ indicates that there must be an error, which can be attributed either to errors in the data processing techniques, or the inability of the models to realistically simulate surface changes due to SMB, firn compaction and/or GIA.

4 Results and discussion

The chosen region is part of a vast area in East Antarctica that shows an increase in mass, suggesting that the ice sheet is growing in this region. The signal the GRACE satellites detect includes changes in mass due to accumulation, ice discharge and GIA. In Figure 3 we show the observed change in mass measured by GRACE. Figure 3a shows the map of the GRACE mass change signal and Figure 3b shows a time series for a coastal location near 67°S 54°E for the entire operational period. In order to obtain the signal that is solely due to ice mass changes the contribution of GIA needs to be removed. In Figure 4 we show the GRACE signal corrected for GIA uplift rates using the ICE-6G_C (VM5) model by Peltier et al. (2015), W12a model by Whitehouse et al. (2012) and the recomputed version

ICE6G_ANU of Purcell et al. (2016), respectively. Using ICE-6G_C (VM5) (Fig. 4a) significantly reduces the observed positive anomaly in Enderby Land, while applying W12a (Fig. 4b) and ICE6G_ANU (Fig. 4c) results in a smaller reduction of the mass anomaly, yielding a similar corrected GRACE signal. Due to the similarity between the W12a and ICE6G_ANU model the W12a model was

5   chosen to correct the satellite observations for GIA, although the effect on the rate of change due to ice dynamic is insignificant between the models due to very small uplift rates across our study region. With the contribution of GIA removed, the signal should only comprise contributions from snowfall and ice discharge. The GIA-corrected GRACE observations suggest a positive anomaly between 30°E and 70°E and a substantial increase in mass between 2003-2009 (Fig. 4b).

10   The modelled trend in SMB and surface elevation due to SMB and firn compaction can now be removed from the GRACE and ICESat observations (Eq. 11 and Eq. 12), to obtain $\frac{dM_{GRACE}^{ice}}{dt}$ and $\frac{dH_{ICESat}^{ice}}{dt}$ and, subsequently, $\frac{dH_{GRACE}^{ice}}{dt}$ and $\frac{dM_{ICESat}^{ice}}{dt}$ by dividing (multiplying) by the density of glacier ice. We converted the rate of change of surface elevation due to the ice dynamic signal obtained from ICESat into spherical harmonics to be comparable with $\frac{dH_{GRACE}^{ice}}{dt}$. By doing this we represent the ice height

15   information with the same spatial resolution as the mass change information, and impose the same potential leakage on to the altimetry observations. The estimated rate of change due to ice dynamics are shown in Figure 5, comparing estimates obtained using two different SMB models: RACMO2.1 and RACMO2.3.

We obtained similar rates of change due to ice dynamic by removing the modelled SMB estimates from

20   both RACMO2 models and GIA uplift rates from GRACE and ICESat observations. Using SMB estimates from RACMO2.3 the ice dynamic estimates are significant smaller and primarily present between 30°E and 60°E with estimated rates between -0.08 to -0.13 m yr^{-1} obtained across the region. Using SMB estimates from RACMO2.1 yields a change due to ice dynamic of -0.08 m yr^{-1} and above along the entire ice sheet margin of our study region, stretching across to 75°E. Generally, using

25   RACMO2.3 the SMB estimates show a smaller difference between the obtained ice dynamic estimates obtained from GRACE and ICESat, improving results across the study area. However, regions remain that exhibit differences in the obtained ice dynamic signal of up to ± 0.05 m yr^{-1} (Fig. 5c and 5f).

13

Significant changes emerge between the rate of change due to ice dynamics obtained using the former and latter RACMO2 versions, with an, over the study region averaged, RMS error of 0.019 m yr^{-1} and 0.021 m yr^{-1} for RACMO2.3 and RACMO2.1, respectively.

In both $\frac{dH^{ice}_{ICESat}}{dt}$ rates a positive trend is estimated across the centre of the region. This is the result of a

5 slightly positive elevation trend that has been recorded by ICESat observations in region D (Fig. 6b). Finally, the total change in surface elevation is modelled, based on dH^{SMB}/dt, dH^{fc}/dt, dH^{GIA}/dt and $\frac{dH^{ice}_{GRACE}}{dt}$ (Fig. 6a). Using RACMO2.3, the result of the modelled rate of change of surface elevation reveals a similar pattern to the ICESat observations (Fig. 6b). In region A both the negative trend between 28°E and 32°E and the positive trend at 34°E is modelled. In region B a general negative trend

10 is recorded along the ice margin with a positive trend near 46°E. Both signals appear in our modelled elevation trend, though at a smaller magnitude. Similarly for region C, which shows a general negative trend across the region, with the lowest trend near 51°E and a strong positive signal at 56°E. While the general negative trend is obtained in the model, the strong negative signal near 51°E is not present. The strong positive signal at 56°E is modelled, although it appears slightly over predicted, covering a larger

15 region than seen in the ICESat observations. Across region D ICESat monitored an overall increase in elevation, especially near 70°E, together with a slight decrease in surface height along the margin between 58°E and 70°E and at the Mellor Glacier (Fig. 1) near 68°E. Similar to the ICESat observations the general positive trend across the region is modelled, together with the positive signal near 70°E, as well as a slight negative trend across the margin. However, the strong negative trend at the Mellor

20 Glacier is lacking, though the region shows a slight negative trend. Although the modelled trend in surface elevation suggests similar behaviour to the altimetry observations, the signal generally appears damped compared to the ICESat observations. This is likely caused by the loss of spatial resolution through the use of degree 80 spherical harmonics (the resolution of the GRACE gravity fields) to remove the ice dynamic signal.

25 Uncertainties are estimated for the satellite observations and models individually, and error propagation is used to obtain the uncertainty of the modelled ice dynamic estimates and modelled surface elevation changes. The uncertainty estimated for the modelled surface elevation trend varies between near zero

14

and ~6 cm yr^{-1} across the interior and along large parts of the ice sheet margins, and up to 12 cm yr^{-1} for the two locations with high SMB rates. The uncertainty of the monthly GRACE solutions are derived following the method of Wahr et al. (2006) and are around 8 mm w.e. yr^{-1} (Fig. 7a), reducing towards the Polar Regions due to denser ground track coverage (Wahr et al., 2006). The uncertainties of the

5   ICESat observations are below 0.05 m yr^{-1} in the interior, where a dense network of ground-tracks exists, and between 0.15 and 0.3 m yr^{-1} along the ice sheet margins due to greater distances between the ground-tracks and steeper slopes along the margins (Hoffmann, 2016) (Fig. 7b).

For both RACMO2 models the overall uncertainty is given as 8% for the grounded ice sheet (Lenaerts et al., 2012; Van Wessem et al., 2014), resulting in an estimated uncertainty of less than 1 cm yr^{-1} in the

10   interior and up to 6 cm yr^{-1} across the high SMB locations proposed in Enderby Land. The firn compaction model contains several error sources. In general, the complex physics of firn densification is still not fully understood, and the density of snow and firn is not well known, introducing large uncertainties into the computations (Sutterley et al., 2014). Error sources include the parameterisations to estimate surface snow density (Eq. 3) and the densification rate (Eq. 4), together with uncertainties

15   within the forcing climate model RACMO2. As the firn compaction model is tuned to fit observations it is difficult to obtain realistic uncertainty estimates. However, following the idea of Helsen et al. (2008) we obtain our error estimate for the firn compaction model by assessing the propagation of the major error sources that affect firn compaction rates. This was done by applying a bias to the accumulation (8%) and temperature (10 K (Reijmer et al., 2005; Maris et al., 2012)), as well as to the surface snow

20   density (±20 kg m^{-3} (Helsen et al., 2008)). The propagation of the errors is calculated to obtain the total uncertainty of the firn compaction model (Fig. 7c). Across most of the study site the uncertainty is estimated to be around ±2-3 cm yr^{-1}. However, at the two locations with the high SMB rates the uncertainty is significantly larger and is estimated to be up to 8 cm yr^{-1}. Uncertainties for GIA models are not provided, as the models are tuned to fit observations and the best-fitting ice sheet history and

25   earth rheology values (e.g. Velicogna and Wahr, 2006). However, uncertainties within our study region are small due to small uplift rates and differences between the models of < 2mm yr^{-1}. Therefore, the error in the modeled GIA signals in our study region are likely to be small.

To estimate the uncertainty of the modelled ice dynamic and modelled surface elevation change, the

propagation of errors of the particular error source is obtained (Fig. 7d and 7e). Depending on the incorporated satellite mission the uncertainty for the modelled rate of change due to ice dynamic is up to 6 cm yr^{-1} (GRACE, Fig. 7d) and up to 30 cm yr^{-1} (ICESat, Fig. 7e), due to the larger error of the ICESat observations. The uncertainty of the modelled elevation change is 0-12 cm yr^{-1} (Fig. 7f), with the greatest error source being the firn compaction model.

5 Conclusion

The rate of change due to ice dynamics can be estimated independently from GRACE and satellite altimetry observations through the removal of GIA signals, SMB and, in the case of altimetry, firn compaction signals. Both approaches depend upon a separate SMB model, although in different ways since SMB causes a mass change in GRACE observations but a height change in altimetry observations. Therefore, any errors in the modelled SMB lead to differences in the ice dynamic estimates derived from GRACE versus altimetry. Thus, this approach provides a new and independent means of assessing the accuracy of SMB models. We showed that the differences between the old and new RACMO2 versions yield significantly different ice dynamic estimates, with RACMO2.3 producing smaller differences between the GRACE- and ICESat-derived estimates.

Although different GIA models affect GRACE and altimetry observations in different ways, changes in GIA models have a small effect on the estimated rate of change due to ice dynamic and so are not responsible for different estimates using the two satellite techniques. Our data suggests that the differences are not based on errors in the ICESat observations as most of the greatest differences occur in regions where ICESat uncertainties are low (Fig. 7c), in particular the large, negative difference occurring inland within the study region (significantly different from zero at the 95% confidence level). Moreover, modelling the rate of change of surface elevation based on ice dynamic estimates obtained from GRACE observations and RACMO2.3 estimates positive and negative changes in elevation in the same regions as ICESat detects corresponding trends, though the rates appear slightly under-estimated compared to the altimetry observations. Therefore, it appears that the dominant driver in the differences of the modelled rate of change due to ice dynamic and surface elevation trends are the changes of the

16

SMB rates within the RACMO2 model, with RACMO2.3 providing a more accurately modelled rate of change of surface elevation. Thus, a comparison of estimated changes in ice dynamics derived from GRACE and altimetry observations not only provides information about dynamic mass changes, but may also help to identify regions where models fail to accurately simulate variations in SMB.

5 Acknowledgement

References

10 Abshire, J. B., Sun, X., Riris, H., Sirota, J. M., McGarry, J. F., Palm, S., Yi, D. and Liiva, P.: Geoscience Laser Altimeter System (GLAS) on the ICESat Mission: On-orbit measurement performance, Geophysical Research Letters, 32(21), L21S02, 2005

Allison, I., Alley, R. B., Fricker, H. A., Thomas, R. H. and Warner, R. C.: Ice sheet mass balance and sea level, Antarctic Science, 21(05), 413-426, 2009

15 Arthern, R. J., Vaughan, D.G., et al.: In situ measurements of Antarctic snow compaction compared with predictions of models, Journal of Geophysical Research, 15306, 2010

Brenner, A. C., DiMarzio, J. P. and Zwally, H. J.: Precision and Accuracy of Satellite Radar and Laser Altimeter Data Over the Continental Ice Sheets, Geoscience and Remote Sensing, IEEE Transactions on, 45(2), 321-331, 2007

20 Bruinsma, S., Lemoine, J.-M., Biancale, R. and Valès, N.: CNES/GRGS 10-day gravity field models (release 2) and their evaluation, Advances in Space Research, 45(4), 587-601, 2010

Cuffey, K. a. P., W. S. B.: The Physics of Glaciers, Elsevier Store, 4th Edn., Pergamon, Oxford, U.K., 2010

Ewert, H., Groh, A. and Dietrich, R.: Volume and mass changes of the Greenland ice sheet inferred

25 from ICESat and GRACE, Journal of Geodynamics, 59-60(0), 111-123, 2012

Gunter, B., Urban, T., Riva, R., Helsen, M., Harpold, R., Poole, S., Nagel, P., Schutz, B. and Tapley, B.: A comparison of coincident GRACE and ICESat data over Antarctica, Journal of Geodesy, 83(11), 1051-1060, 2009

Helsen, M. M., van den Broeke, M. R., van de Wal, R. S. W., van de Berg, W. J., van Meijgaard, E.,
5 Davis, C. H., Li, Y. and Goodwin, I.: Elevation Changes in Antarctica Mainly Determined by Accumulation Variability, Science, 320(5883), 1626-1629, 2008

Herron, M., and Langway, C.: Firn Densification: An emperical model, Journal of Glaciology, 251980

Hoffmann, J.: Ice height changes in East Antarctica derived from satellite laser altimetry, The Australian National University, PhD Thesis, 2016

10 Horwath, M., Lemoine, J.-M., Biancale, R. and Bourgogne, S.: Improved GRACE science results after adjustment of geometric biases in the Level-1B K-band ranging data, Journal of Geodesy, 85(1), 23-38, 2011

Kaspers, K. A., van de Wal, R. S. W., van den Broeke, M. R., Schwander, J., van Lipzig, N. P. M. and Brenninkmeijer, C. A. M.: Model calculations of the age of firn air across the Antarctic continent,
15 Atmos. Chem. Phys., 4(5), 2004

Kuipers Munneke, P., Ligtenberg, S. R. M., Suder, E. A. and Van Den Broeke, M. R.: A model study of the response of dry and wet firn to climate change, Annals of Glaciology, 56(70), 1-8, 2015

Legresy, B., Papa, F., Remy, F., Vinay, G., van den Bosch, M. and Zanife, O.-Z.: ENVISAT radar altimeter measurements over continental surfaces and ice caps using the ICE-2 retracking algorithm,
20 Remote Sensing of Environment, 95(2), 150-163, 2005

Lemoine, J.-M., Bruinsma, Sean, Gégout, Pascal, Biancale, Richard, Bourgogne, Stéphane: Release 3 of the GRACE gravity solutions from CNES/GRGS, Geophysical Research Abstracts, 15(EGU2013-11123), 2013

Lenaerts, J. T. M. and van den Broeke, M. R.: Modelling drifting snow in Antarctica with a regional
25 climate model: 2. Results, Journal of Geophysical Research: Atmospheres, 117(D5), D05109, 2012

Lenaerts, J. T. M., van den Broeke, M. R., van de Berg, W. J., van Meijgaard, E. and Kuipers Munneke, P.: A new, high-resolution surface mass balance map of Antarctica (1979–2010) based on regional atmospheric climate modelling, Geophysical Research Letters, 39(4), L04501, 2012

Ligtenberg, S. R. M., Helsen, M.M. and van den Broeke, M.R.: An improved semi-emperical model for the densification of Antarctic firn, The Cryosphere, 5809-819, 2011

Ligtenberg, S. R. M., Medley, B., Van Den Broeke, M. R. and Munneke, P. K.: Antarctic firn compaction rates from repeat-track airborne radar data: II. Firn model evaluation, Annals of Glaciology,
5   56(70), 167-174, 2015

Maris, M. N. A., de Boer, B. and Oerlemans, J.: A climate model intercomparison for the Antarctic region: present and past, Clim. Past, 8(2), 803-814, 2012

Mouginot J., B. S. a. E. R.: Mapping of Ice Motion in Antarctica Using Synthetic-Aperture Radar Data, Remote Sensing, doi 10.3390/rs4092753 2012

10   Pagiatakis, S. D.: The response of a realistic earth to ocean tide loading, Geophysical Journal International, 103(2), 541-560, 1990

Peltier, W. R., Argus, D. F. and Drummond, R.: Space geodesy constrains ice age terminal deglaciation: The global ICE-6G_C (VM5a) model, Journal of Geophysical Research: Solid Earth, 120(1), 450-487, 2015

15   Pritchard, H. D., Arthern, R. J., Vaughan, D. G. and Edwards, L. A.: Extensive dynamic thinning on the margins of the Greenland and Antarctic ice sheets, Nature, 461(7266), 971-975, 2009

Purcell, A., Dehecq, A. et al.: Relationship between glacial isostatic adjustment and gravity perturbations observed by GRACE, Geophys. Res. Lett., 38, 2011

Purcell, A., Tregoning, P. and Dehecq, A.: An assessment of the ICE6G_C(VM5a) glacial isostatic
20   adjustment model, Journal of Geophysical Research: Solid Earth, 121(5), 3939-3950, 2016

Reijmer, C. H., van Meijgaard, E. and van den Broeke, M. R.: Evaluation of temperature and wind over Antarctica in a Regional Atmospheric Climate Model using 1 year of automatic weather station data and upper air observations, J. Geophys. Res., 110(D4), D04103, 2005

Rémy, F., Flament, T., Michel, A. l. and Verron, J.: Ice sheet survey over Antarctica using satellite
25   altimetry: ERS-2, Envisat, SARAL/AltiKa, the key importance of continuous observations along the same repeat orbit, International Journal of Remote Sensing, 35(14), 5497-5512, 2014

Rémy, F. and Frezzotti, M.: Antarctica ice sheet mass balance, Comptes Rendus Geosciences, 338(14-15), 1084-1097, 2006

Rignot, E.: Changes in ice dynamics and mass balance of the Antarctic ice sheet, Philosophical Transactions of the Royal Society A: Mathematical, Physical and Engineering Sciences, 364(1844), 1637-1655, 2006

Rignot, E., Bamber, J. L., van den Broeke, M. R., Davis, C., Li, Y., van de Berg, W. J. and van Meijgaard, E.: Recent Antarctic ice mass loss from radar interferometry and regional climate modelling, Nature Geosci, 1(2), 106-110, 2008

Rignot, E., J. Mouginot, and B. Scheuchl: MEaSUREs InSAR-Based Antarctica Velocity Map, Boulder, Colorado USA: NASA EOSDIS Distributed Active Archive Center at NSIDC, Accessed on (03/04/2015). http://nsidc.org/data/nsidc-0484.html2011

Rignot, E., Jacobs, S., Mouginot, J. and Scheuchl, B.: Ice-Shelf Melting Around Antarctica, Science, 341(6143), 266-270, 2013

Rignot, E. and Thomas, R. H.: Mass Balance of Polar Ice Sheets, Science, 297(5586), 1502-1506, 2002

Sasgen, I., Konrad, H., Ivins, E. R., Van den Broeke, M. R., Bamber, J. L., Martinec, Z. and Klemann, V.: Antarctic ice-mass balance 2003 to 2012: regional reanalysis of GRACE satellite gravimetry measurements with improved estimate of glacial-isostatic adjustment based on GPS uplift rates, The Cryosphere, 7(5), 1499-1512, 2013

Shepherd, A., Ivins, E. R., A, G., Barletta, V. R., Bentley, M. J., Bettadpur, S., Briggs, K. H., Bromwich, D. H., Forsberg, R., Galin, N., Horwath, M., Jacobs, S., Joughin, I., King, M. A., Lenaerts, J. T. M., Li, J., Ligtenberg, S. R. M., Luckman, A., Luthcke, S. B., McMillan, M., Meister, R., Milne, G., Mouginot, J., Muir, A., Nicolas, J. P., Paden, J., Payne, A. J., Pritchard, H., Rignot, E., Rott, H., Sørensen, L. S., Scambos, T. A., Scheuchl, B., Schrama, E. J. O., Smith, B., Sundal, A. V., van Angelen, J. H., van de Berg, W. J., van den Broeke, M. R., Vaughan, D. G., Velicogna, I., Wahr, J., Whitehouse, P. L., Wingham, D. J., Yi, D., Young, D. and Zwally, H. J.: A Reconciled Estimate of Ice-Sheet Mass Balance, Science, 338(6111), 1183-1189, 2012

Slobbe, D. C., Lindenbergh, R.C. and Ditmar, P.: Estimation of volume change rates of Greenland's ice sheet from ICESat data using overlapping footprints, Remote Sensing of Environment, 112, 2008

Sørensen, L. S., Simonsen, S.B., et al.: Mass balance of the Greenland ice sheet (2003-2008) from ICESat data-the impact of interpolation, sampling and firn density, The Cryosphere, 5173-186, 2011

20

Sutterley, T. C., Velicogna , I., Csatho , B., van den Broeke, M., Rezvan-Behbahani, S. and Babonis, G.: Evaluating Greenland glacial isostatic adjustment corrections using GRACE, altimetry and surface mass balance data, Environmental Research Letters, 9(1), 014004, 2014

Tapley, B. D., Bettadpur, S., Watkins, M. and Reigber, C.: The gravity recovery and climate
5   experiment: Mission overview and early results, Geophys. Res. Lett., 31(9), L09607, 2004

Van Wessem, J. M., Reijmer, C. H., Morlighem, M., Mouginot, J., Rignot, E., Medley, B., Joughin, I., Wouters, B., Depoorter, M. A., Bamber, J. L., Lenaerts, J. T. M., Van De Berg, W. J., Van Den Broeke, M. R. and Van Meijgaard, E.: Improved representation of East Antarctic surface mass balance in a regional atmospheric climate model, Journal of Glaciology, 60(222), 761-770, 2014

10   Velicogna, I.: Increasing rates of ice mass loss from the Greenland and Antarctic ice sheets revealed by GRACE, Geophysical Research Letters, 36(19), L19503, 2009

Velicogna, I. and Wahr, J.: Measurements of Time-Variable Gravity Show Mass Loss in Antarctica, Science, 311(5768), 1754-1756, 2006

Wahr, J., Molenaar, M. and Bryan, F.: Time variability of the Earth's gravity field: Hydrological and
15   oceanic effects and their possible detection using GRACE, J. Geophys. Res., 103(B12), 30205-30229, 1998

Wahr, J., Swenson, S. and Velicogna, I.: Accuracy of GRACE mass estimates, Geophys. Res. Lett., 33(6), L06401, 2006

Whitehouse, P. L., Bentley, M. J., Milne, G. A., King, M. A. and Thomas, I. D.: A new glacial isostatic
20   adjustment model for Antarctica: calibrated and tested using observations of relative sea-level change and present-day uplift rates, Geophysical Journal International, 190(3), 1464-1482, 2012

Zwally, H. J., Giovinetto, M.B., Li, J., Cornejo, H.G., Beckley, M.A., Brenner, A.C., Saba, J.L., Yi, D.: Mass changes of the Greenland and Antarctic ice sheets and shelves and contributions to sea-level rise: 19922002, Journal of Glaciology, 51509-527, 2005

25   Zwally, H. J. and Li, J.: Seasonal and interannual variations of firn densification and ice-sheet surface elevation at the Greenland summit, Journal of Glaciology, 48(161), 199-207, 2002

Zwally, H. J., Schutz, B. et al.: ICESat's laser measurements of polar ice, atmosphere, ocean and land, Journal of Geodynamics, 34405-445, 2002

21

| SMB (kg m^{-2} yr^{-1})	alpha	beta
<100	1.00	1.00
100-300	0.96	0.97
300-500	0.93	0.94
500-700	0.92	0.93
700-1000	0.90	0.86
1000-2500	0.88	0.86
2500-4000	0.87	0.84
>4000	0.87	0.54

Table A1:

5 **Proposed values for the accumulation constants α and β used in our monthly firn compaction model. The constants are dependent on the accumulation rate and have been adapted to a best-fit.**
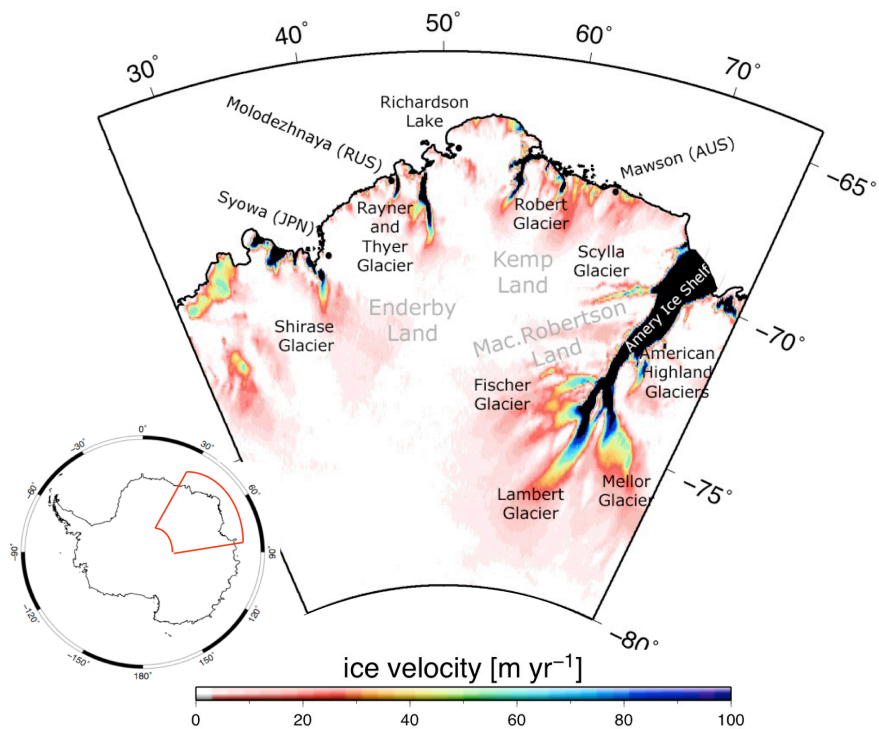
Figure 1: Regional map of our study area including Enderby Land, Kemp Land and Mac.Robertson Land. The map includes the locations of permanent research stations and major outlet glaciers. Ice velocity rates are plotted, sourced from the NASA MEaSUREs program (Rignot et al., 2011; Mouginot et al., 2012), to identify glaciers and regions with dynamic ice loss.

5

23
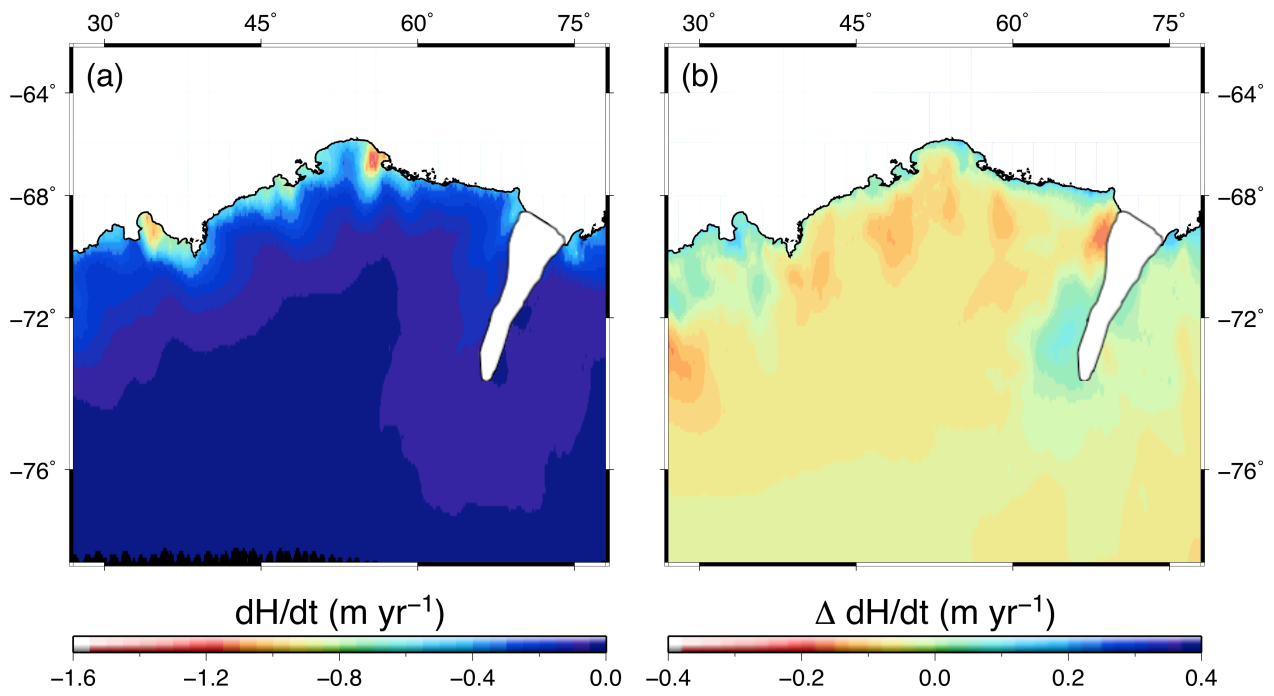
Figure 2: (a) Average annual vertical velocity rates due to firn compaction across the study site as obtained from our monthly firn compaction model, and **(b)** the differences between our model results and the firn densification model of Ligtenberg et al. (2011).
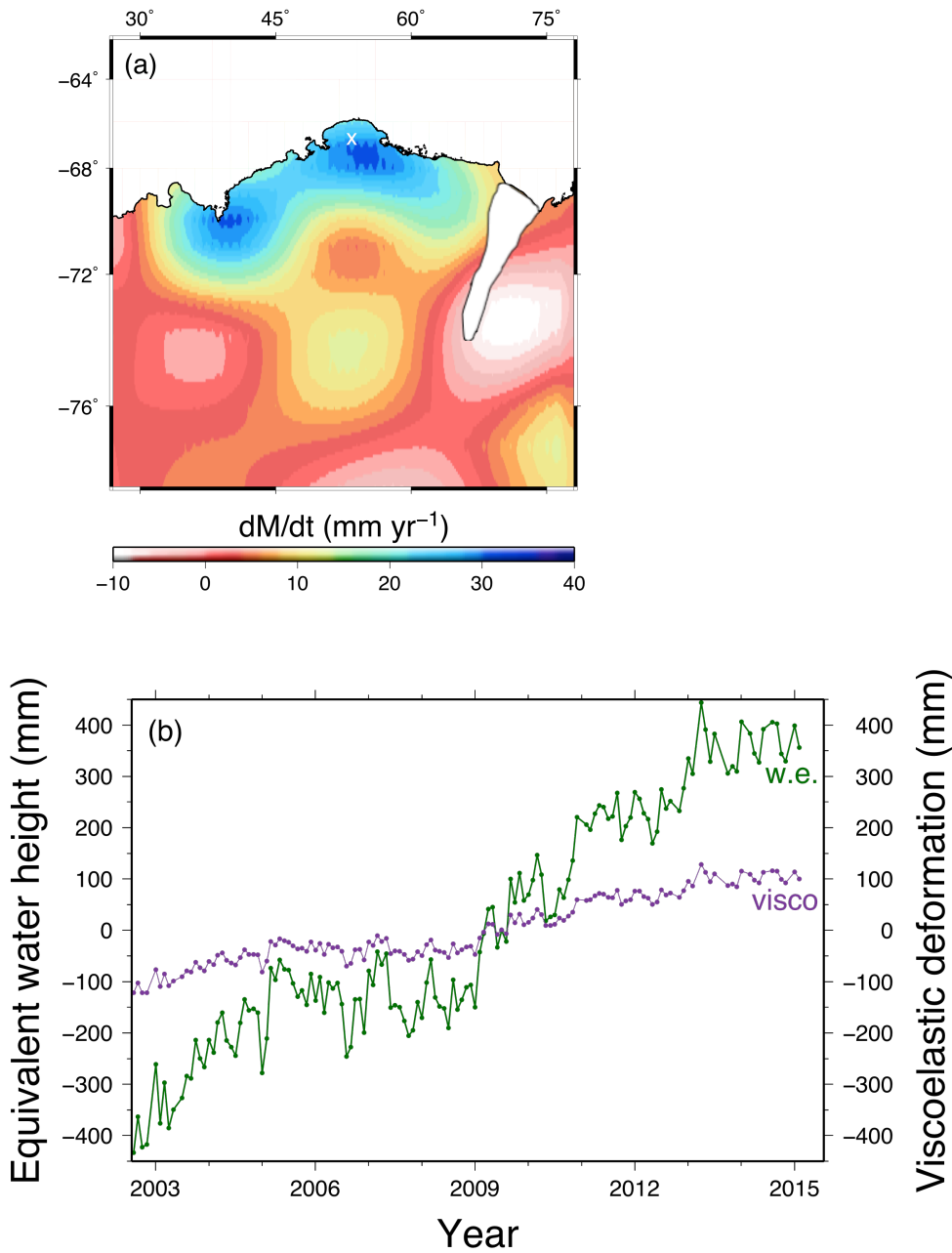
Figure 3: (a) Trend of the observed mass anomalies in Enderby Land monitored by GRACE over the time span of 2003-2009, uncorrected for GIA. The white cross illustrates the location of Richardson Lake, a former GPS station. **(b)** The time series shows a change in gravity at a chosen location in Enderby Land (67S 54E) over the total observational period. The green line illustrates the change assuming the gravitational change is caused by a surface mass load and is expressed in water equivalent (w.e.) (Eq.1), the purple line illustrates a change due to viscoelastic deformation (GIA) (Eq.2).
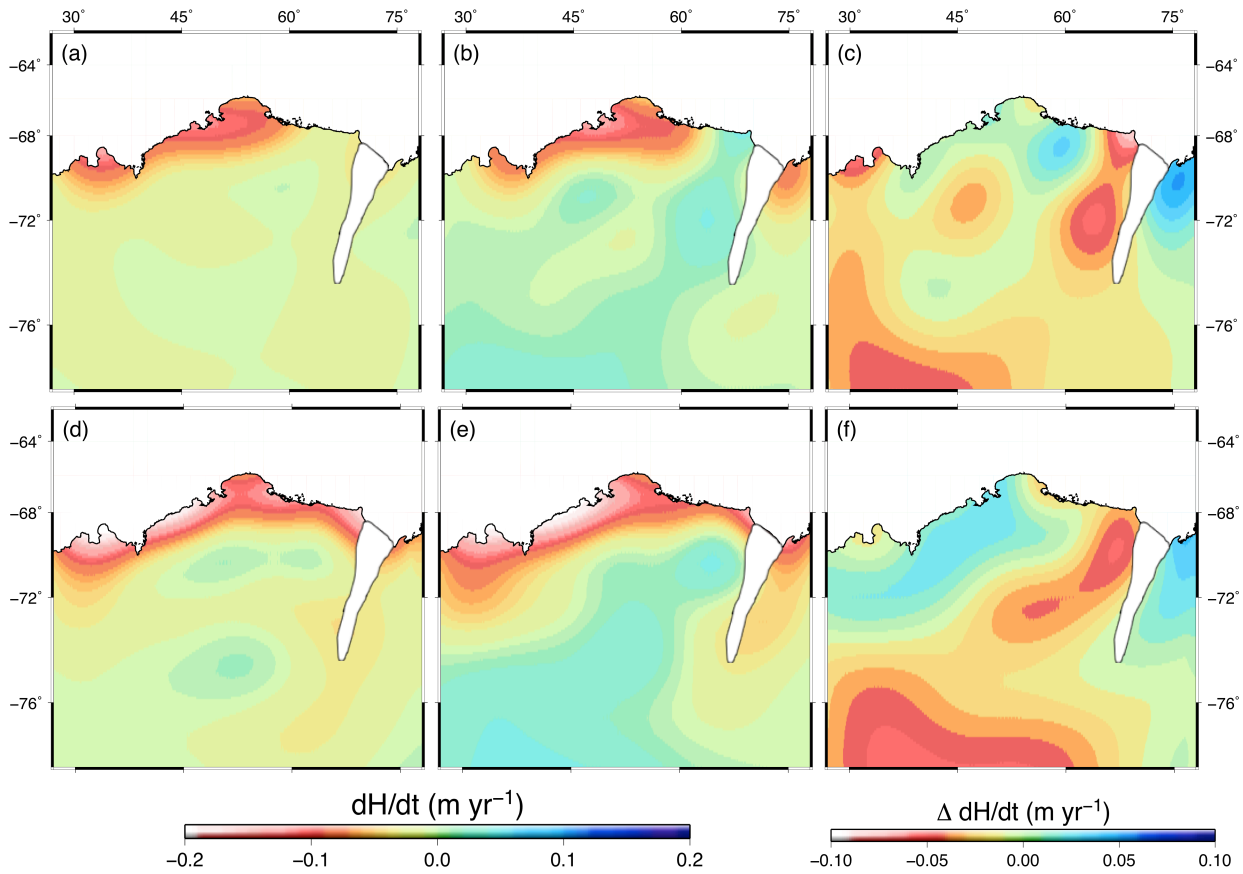
5

10
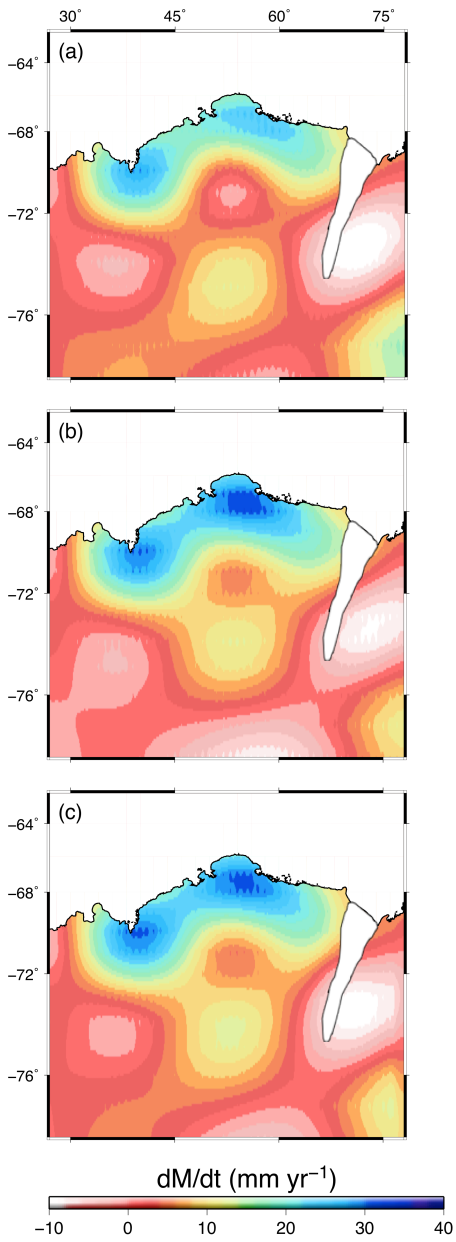
Figure 4: GRACE observations corrected for GIA uplift rates using (a) the ICE-6G_C(VM5) model by Peltier et al (2015), (b) the W12a model by Whitehouse et al. (2012), and (c) the ICE6G_ANU model by Purcell et al. (2016).

26

Figure 5: Comparison between the modelled ice dynamic rates obtained by employing SMB estimates from RACMO2.3 using (a) GRACE and (b) ICESat, and by employing SMB estimates from RACMO2.1 using (d) GRACE and (e) ICESat. (c) and (f) show the difference between ice dynamic rates obtained from GRACE minus ice dynamic rates obtained from ICESat for the employed SMB estimates obtained from RACMO2.3/ANT and RACMO2.1/ANT, respectively.
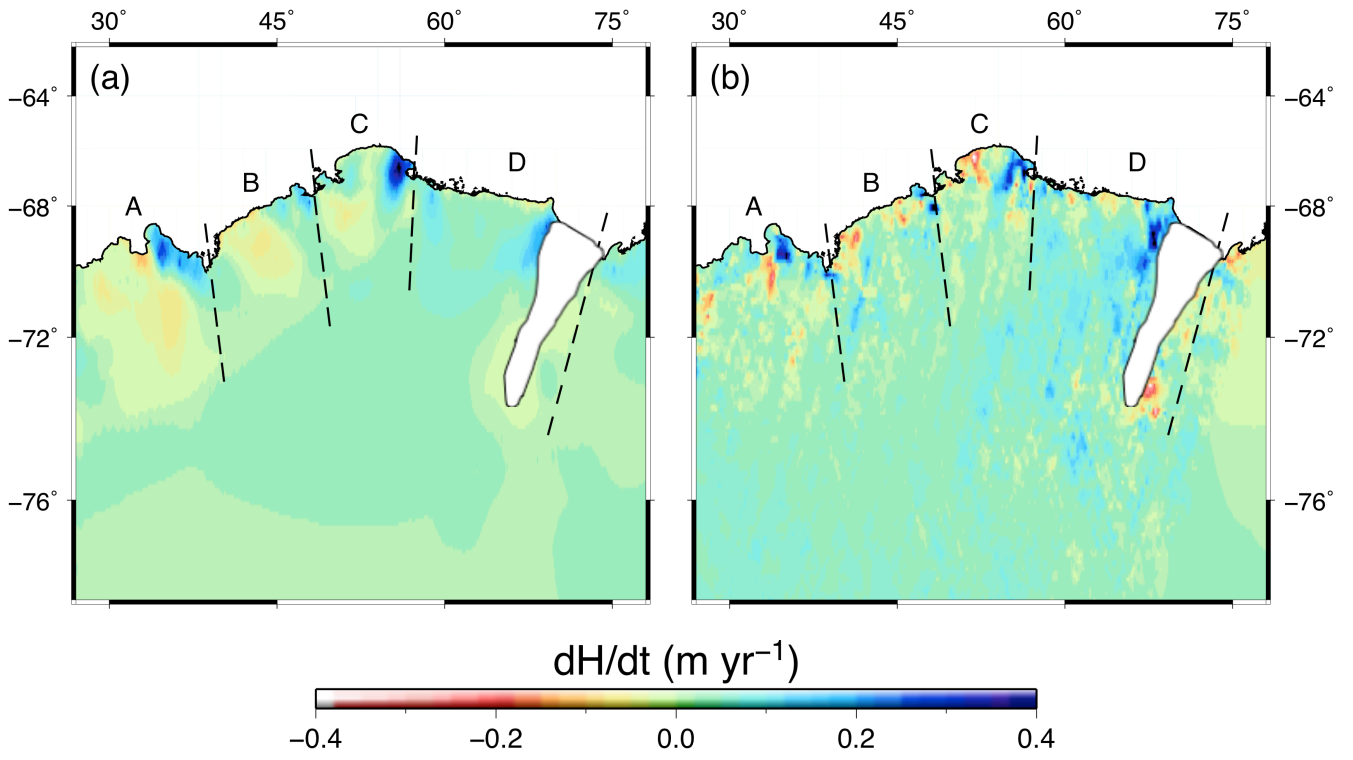
27

Figure 6: (a) our modelled rate of change of surface elevation retrieved by removing our estimated ice dynamic rates, obtained from GRACE, from the modelled trend in surface elevation (SMB-firn compaction) using RACMO2.3, compared to (b) the ICESat observations.
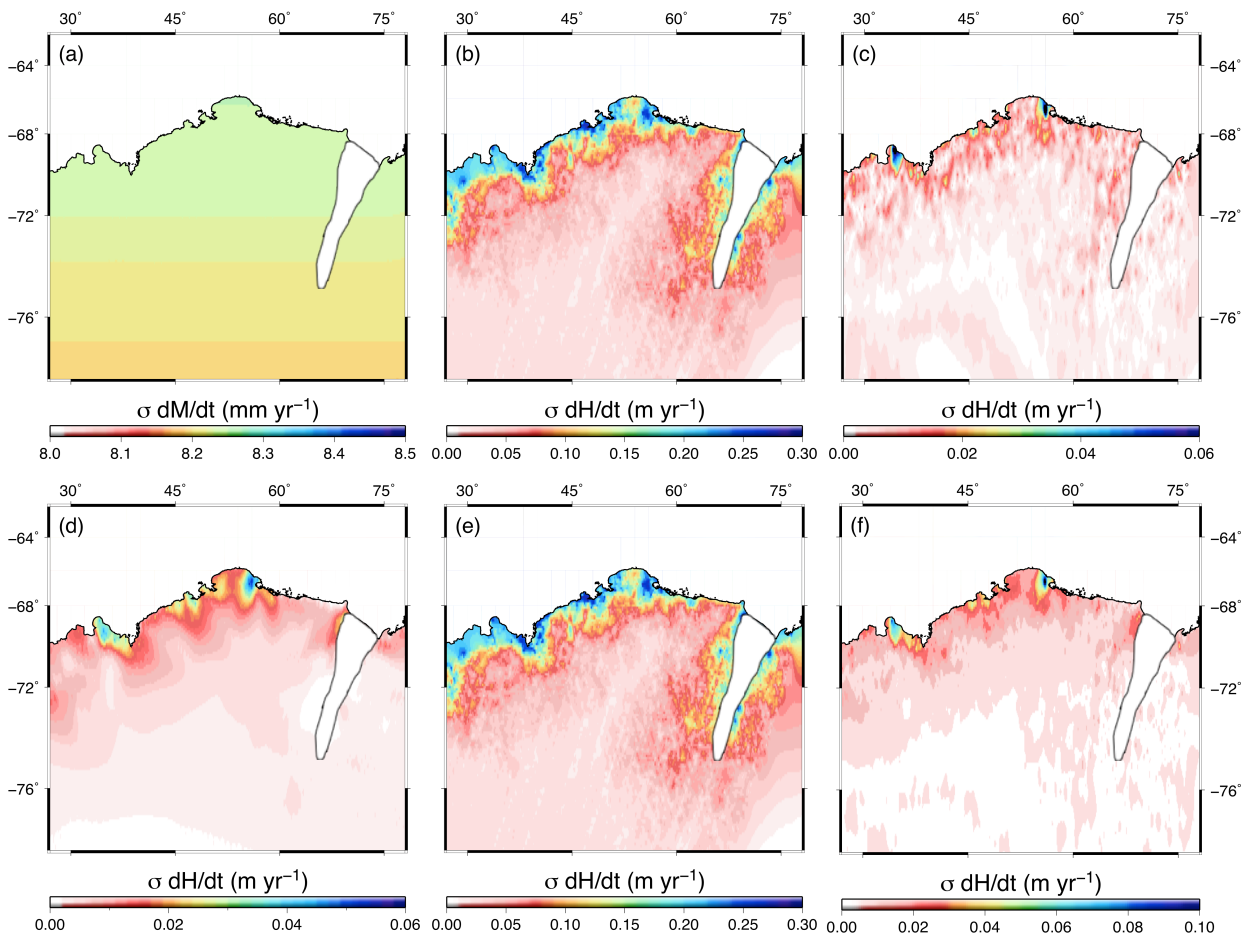
28

Figure 7: Uncertainties estimated for (a) GRACE, (b) ICESat, (c) our monthly firn compaction model, ice dynamic rates using RACMO2.3 obtained from (d) GRACE, (e) ICESat, and the modelled surface elevation trend for (f) RACMO2.3. The greatest uncertainty comes from the ICESat measurements, with up to 30 cm yr⁻¹ at the margins, this results in greater uncertainties for the modelled ice dynamic rates obtained from the ICESat observations.

29